AFRL-AFOSR-JP-TR-2016-0071

Controlled Interactions between Two Dimensional Layered Inorganic Nanosheets and Polymers

Cheolmin Park
YONSEI UNIVERSITY UNIVERSITY-INDUSTRY FOUNDATION

06/15/2016
Final Report

Air Force Research Laboratory
AF Office Of Scientific Research (AFOSR)/ IOA
Arlington, Virginia 22203
Air Force Materiel Command

REPORT DOCUMENTATION PAGE

Form Approved
OMB No. 0704-0188

1. REPORT DATE *(DD-MM-YYYY)*	2. REPORT TYPE	3. DATES COVERED *(From - To)*
15-06-2016	Final	03 Sep 2014 to 02 Sep 2015

4. TITLE AND SUBTITLE
Controlled Interactions between Two Dimensional Layered Inorganic Nanosheets and Polymers

5a. CONTRACT NUMBER

5b. GRANT NUMBER
FA2386-14-1-4054

5c. PROGRAM ELEMENT NUMBER
61102F

6. AUTHOR(S)
Cheolmin Park

5d. PROJECT NUMBER

5e. TASK NUMBER

5f. WORK UNIT NUMBER

7. PERFORMING ORGANIZATION NAME(S) AND ADDRESS(ES)
YONSEI UNIVERSITY UNIVERSITY-INDUSTRY FOUNDATION
50 Yonsei-ro, Seodaemun-g
SEOUL, 120-749 KR

8. PERFORMING ORGANIZATION REPORT NUMBER

9. SPONSORING/MONITORING AGENCY NAME(S) AND ADDRESS(ES)
AOARD
UNIT 45002
APO AP 96338-5002

10. SPONSOR/MONITOR'S ACRONYM(S)
AFRL/AFOSR IOA

11. SPONSOR/MONITOR'S REPORT NUMBER(S)
AFRL-AFOSR-JP-TR-2016-0071

12. DISTRIBUTION/AVAILABILITY STATEMENT
A DISTRIBUTION UNLIMITED: PB Public Release

13. SUPPLEMENTARY NOTES

14. ABSTRACT
Layered inorganic materials (LIMs) such as transition metal dichalcogenides (TMDs) (eg., MoS2, WS2, MoSe2, ZrTe2), transition metal oxides (TMOs) (eg. Ti oxides, Nb oxides) and boron nitride (BN) have been of great attraction due to their unique structures and intriguing properties. The layer-dependent properties of LIMs varying from topological insulators to wide-gap semiconductors and metals have endow exciting prospects for a variety of emerging applications in a broad range of fields, such as electronics, energy conversion and storage, catalysis and polymer nanocomposites (PNCs). In particular, the preparation of PNCs with good dispersion of LIM nanosheets within the polymer matrix is of prime importance to realize the intrinsic properties of individual sheets of LIM. In this report, we demonstrate the physical and chemical interactions of two-dimensional nanosheets of LIMs with polymers with the emphasis on controlling the interactions by designing the molecular and architectural structures of the polymers for potential practical applications such as nanocomposites and thin film fabrications. Our approaches are based on the modification of LIMs with end-functionalized polymers. First, an end-functionalized polymer with conjugated end-molecule, pyrene, is successfully employed to boron nitride nanosheets (BNNS), and non-covalent interaction arising from pi-pi interaction gives rise to well dispersed BNNS with high concentration. Second, the non-destructive modification of TMDs sheets with amine-terminated polymers is introduced and the strong Lewis acid-base interaction between transition metal and non-pair electrons of amine allows us to develop scalable, stable and uniform composite films with numerous combinations of TMD nanosheets and end-functionalized polymers.

15. SUBJECT TERMS
2D Materials, Nanosheets, Layered Materials, Nanocomposites

16. SECURITY CLASSIFICATION OF:			17. LIMITATION OF ABSTRACT	18. NUMBER OF PAGES	19a. NAME OF RESPONSIBLE PERSON
a. REPORT	b. ABSTRACT	c. THIS PAGE			CASTER, KENNETH
Unclassified	Unclassified	Unclassified	SAR	23	19b. TELEPHONE NUMBER *(Include area code)* 315-229-3326

Standard Form 298 (Rev. 8/98)
Prescribed by ANSI Std. Z39.18

Final Report for AOARD Grant 14IOA043-144054 "Controlled Interactions between Two Dimensional Layered Inorganic Nanosheets and Polymers"

02 NOV 2015

Prof. Cheolmin Park
Department of Materials Science & Engineering, Yonsei University
50 Yonsei-ro, Seodaemun-gu, Seoul 120-749, Korea
Tel: +85-2-212-2833
Fax: +82-2-312-5375
E-mail: cmpark@yonsei.ac.kr

Period of Performance: SEP/3/2014 – SEP/2/2015

1. Abstract: Layered inorganic materials (LIMs) such as transition metal dichalcogenides (TMDs) (eg.MoS_2, WS_2, $MoSe_2$, $ZrTe_2$), transition metal oxides (TMOs) (eg. Ti oxides, Nb oxides) and boron nitride (BN) have been of great attraction due to their unique structures and intriguing properties. The layer-dependent properties of LIMs varying from topological insulators to wide-gap semiconductors and metals have endow exciting prospects for a variety of emerging applications in a broad range of fields, such as electronics, energy conversion and storage, catalysis and polymer nanocomposites (PNCs). In particular, the preparation of PNCs with good dispersion of LIM nanosheets within the polymer matrix is of prime importance to realize the intrinsic properties of individual sheets of LIM. In this report, we demonstrate the physical and chemical interactions of two-dimensional nanosheets of LIMs with polymers with the emphasis on controlling the interactions by designing the molecular and architectural structures of the polymers for potential practical applications such as nanocomposites and thin film fabrications. Our approaches are based on the modification of LIMs with end-functionalized polymers. First, an end-functionalized polymer with conjugated end-molecule, pyrenes, is successfully employed to boron nitride nanosheets (BNNS), and non-covalent interaction arising from π-π interaction gives rise to well dispersed BNNS with high concentration. Second, the non-destructive modification of TMDs sheets with amine-terminated polymers is introduced and the strong Lewis acid-base interaction between transition metal and non-pair electrons of amine allows us to develop scalable, stable and uniform composite films with numerous combinations of TMD nanosheets and end-functionalized polymers.

2. Introduction.

Research objectives: This research aims to study the physical (van der Waals forces: crystal epitaxy and π-π interaction) and chemical (acid-base force) interactions of two-dimensional nanosheets of layered inorganic materials (LIMs) with polymers with the emphasis on controlling the interactions by designing the molecular and architectural structures of the polymers for potential practical applications such as nanocomposites and thin film fabrications.

Background: LIMs exist in three dimensional forms as stacks of two constituent dimensional layers with strong in-plane covalent bond and weak out-of-plane interactions between the layers. The layer-dependent properties of LIMs such as transition metal dichalcogenides (TMDs) (eg. MoS_2, WS_2, $MoSe_2$, $ZrTe_2$), transition metal oxides (TMOs) (eg.Ti oxides, Nb oxides) and boron

nitride (BN) varying from topological insulators to wide-gap semiconductors and metals have endow exciting prospects for a variety of emerging applications in a broad range of fields, such as electronics, energy conversion and storage, catalysis and polymer nanocomposites. In particular, the impressive and extraordinary mechanical, electrical and barrier properties of LIMs make them attractive as nanofillers to reinforce polymers to prepare multifunctional composites. The preparation of polymer nanocomposites (PNC) with good dispersion of LIM nanosheets within the polymer matrix is of prime importance to realize the intrinsic properties of individual sheets of LIM. In general, the dispersion is, however, very difficult due to high stacking of layers in agglomerated states which make them incompatible with most of the polymers. In addition, no specific chemical interaction between polymers and LIMs hinders the exfoliation and thus development of highly dispersed LIM sheets in polymers remains great challenge, which requires more fundamental understanding of the interaction between LIMs and polymers. Further control of the interaction based on this understanding will offer fruitful opportunities for utilizing emerging LIMs

Importance: To achieve stable exfoliation of LIM nanosheets in different solvents and polymer matrixes, without disrupting the structural integrity, the nature of the interaction between polymer and LIM should be understood and appropriate materials design including chain conformations, site selective chemical structures and molecular architectures of polymers should be made for promoting the interaction with the LIMs. The effective exfoliation of LIMs should be accompanied with favorable attraction of polymer segments on the surface of LIMs which overcomes self-layer-layer van der Waal's attraction of LIM. Beside this enthalpic interaction, sufficient physical separation between two layers should be guaranteed with entropically driven polymer chains to avoid re-aggregation of the layers. The successful manipulation the LIM nanosheets by polymers, therefore, mainly relies upon understanding their physical and chemical interactions with the polymer and furthermore rational design of polymers to control both segmental enthalpic and conformational entropic contributions to the total free energy at the same time

Ultimate goal: There is the necessity to produce large quantities of highly exfoliated LIMs uniformly distributed in polymer matrix with their intrinsic properties maintained to fully harness the desired properties for further practical applications. By analogy with graphene which has been extensively studied for effective separation to individual layers in liquid state, liquid phase exfoliation of LIMs by polymers will advance the development of PNCs. This method brings considerable advantages; long and flexible chains of the polymers can readily adhere to the surface of sheets when the interaction between polymer and sheet properly controlled. In addition, extended polymer chains from the sheets can be readily entangled with other chains of the matrix polymer, thereby ensuring homogeneous PNC formation. The solvent medium offers an extra driving force for mixing between layers and the matrix. In addition, solution processes such as spin coating, dip coating and layer-by-layer coating are in great demand for fabricating thin films with the thickness of a few hundred nanometers or less, such thin films can in turn be readily combined with various thin film electronic, optic and mechanical applications.

3. Experiment

3-1) LIMs / pyrene-terminated polymer

Materials: Stacked *h*-boron nitride (BN) was purchased from Alpha Aesar. Molybdenum disulfide (MoS_2), *N*,*N*-dimethtyl formamide (DMF), 1-pyrenemethanol, 4-vinylpyridine (4-VP), 4-cyano-4-[(dodecylsulfanylthiocarbonyl)sulfanyl]pentanoic acid, 4-(dimethylamino)pyridine (DMAP), 2,2-azobis(2-methylpropionitrile) (AIBN) and dicyclohexylcarbodiimide (DCC) were purchased from Sigma-Aldrich. *N*-butoxycarbonylhydrazine-1,4-butanediamine (C4-Boc) was purchased from TCI. AIBN was used after precipitating in the cold methanol and 4-VP was purified with basic aluminum oxide and vacuum distillation. The others were used as received.

Polymerization of poly(4-vinylpyridine) (P4VP) derivatives: The pyrene-terminated poly(4-vinlypyridine) (P4VP-Py), 1,4-butanediamine-terminated poly(4-vinlypyridine) (P4VP-C4-amine) and *N*-butoxycarbonylhydrazine-1,4-butanediamine-terminated poly(4-vinlypyridine) (P4VP-C4-Boc) were functionalized from P4VP chain as shown in **Figure 1**. P4VP was polymerized by RAFT where 4-cyano-4-[(dodecylsulfanylthiocarbonyl)sulfanyl] pentanoic acid and AIBN were used as chain transfer agent (CTA) and initiator, respectively. The mixtures (Monomer : CTA : initiator = 200 : 1 : 0.1) and small amount of DMF were charged in a round-bottom flask, subsequently the solution was conducted by 3 times with freeze-pump thaw. After reacting in coil-bath for 1day at 68 °C, the crude was precipitated by the co-solvent with ether and *n*-hexane. The yellow powder of P4VP (M_w: 16 kg/mole and PDI: 1.16) was analyzed by gel permeation chromatography (GPC). Note that functionalization of end group can be achieved by DCC coupling from a carboxylic acid-terminated P4VP according to the RAFT mechanism. The 1-pyrenemethanol and C4-Boc were used for functionalization of P4VP-Py and P4VP-C4-Boc, respectively. The *N*-butoxycarbonylhydrazine (Boc) group of P4VP-C4-Boc was additionally removed by triflouroacetic acid (TFA) for preparing P4VP-C4-amine.

Exfoliation & Dispersion: To exfoliate and disperse the BN or MoS_2, P4VP-Py was firstly dissolved in DMF (2 mg/ml). Next, ultra-sonication was performed in the iced bath with 50 % of the power for 2 h. After waiting for 1 day to remove the precipitated part, we centrifuged supernatant under 1200 rpm for 30 min.

Characterization: To confirm the amount differences of the dispersed MoS_2, UV-vis spectroscopy (Lamda 750 spectrometer, Perkin-Elmer) was evaluated with 20 times diluted solution.

3-2) TMDs / end-functionalized polymers.

3-2.1) TMDs with mono-end-functionalized polymers

Materials: TMD powders were purchased from Alfa Aeser and Sigma Aldrich. The amine-terminated polymers: polystyrene (PS-NH_2) (9.5~108 kg/mol), polyethylene oxide (PEO-NH_2) (9.5 kg/mol), poly(methyl methacrylate) (PMMA-NH_2) (20 kg/mol), polybutadiene (PBd-NH_2) (15 kg/mol), polyethylene (PE-NH_2) (4.2 kg/mol) and poly(styrene-*b*-isoprene) (PS-*b*-PI-NH_2) (23-*b*-37.5 kg/mol), and polystyrene (PS) (11.5 kg/mol) homopolymer were procured from Polymer Source Inc., Doval, Canada. The detail physical properties of the polymers and TMD powders are listed in the **Tables 1 and 2**, respectively. All of the solvents

were purchased from Sigma Aldrich.

Exfoliation & Dispersion: In a typical procedure, 250 mg of bulk $MoSe_2$ powder and 25 mg of PS-NH_2 were added into a 30-ml glass vial containing 25 ml of toluene. The solution was sonicated for 45 min by using a tip sonicator with a 10-s On pulse and a 5-s OFF pulse at an amplitude of 50% in an ice bath. The dispersions were allowed to settle for 24 h, and then the top dispersion was decanted and centrifuged for 30 min at 1,500 rpm to remove the unexfoliated and large particles. After centrifugation, the top half of the dispersion was collected and the concentration of $MoSe_2$ nanosheets was determined by standard gravimetric analysis.

Film Preparation: (1) $MoSe_2$ with various amine-terminated polymers such as PEO-NH_2, PMMA-NH_2, PBd-NH_2, PE-NH_2 and PS-*b*-PI-NH_2, and (2) PS-NH_2 based composite films containing various TMDs including MoS_2, WS_2, ReS_2, WSe_2, $ZrTe_2$ and $NbSe_2$ were fabricated by spin-coating on a Si substrate.

Simulation method: The model systems are constructed by generating a chain molecule under interest on a 5x3 rectangular 1T-TiS_2 supercell with toluene molecules, where the density of molecules in the simulation cell is set to be 1.2 g/cm^3 to approximate PS/TiS_2 in toluene. The geometry optimization of the model system was performed according to density functional tight binding (DFTB) theory using DFTB+ package with the tiorg and mio parameter set and UFF-based dispersion corrections. The optimized systems were then equilibrated by DFTB-MD simulation in NVT ensemble at 298 K for 10 ps. The concentration profiles were obtained from the time averaging of MD samples for extra 5 ps run after the equilibration.

Characterization: A horn probe tip sonicator (VibraCell CVX;750 W) was used to exfoliate the TMDs with amine-terminated polymers. Centrifugation was carried out using a Hettich Mikro 22R centrifuge. The optical absorbance spectra were measured by ultraviolet-visible-NIR spectrophotometer (JASCO V-530) using 1-cm quartz cuvettes. FT-IR studies were performed using a JASCO FT-IR 300E apparatus (Tokyo, Japan) with KBr as a standard. The thermogravimetric analysis (TGA) of the samples was carried out using a TA Q500 thermal analyser at a heating rate of 10-Cmin-1 under a nitrogen atmosphere. X-ray photoelectron spectroscopy (K-alpha Thermo VG, .K.) measurements were acquired using a monochromated Al X-ray source (Al Ka line: 1486.6 eV). Raman and PL measurements (LabRamAramis) were carried out using a 532-nm laser at a power of 0.5mW and an exposition time of 10 s. X-ray diffraction patterns were recorded using a Dmax/2500-H (Rigaku, Japan). The nanostructures of the TMDs were examined by tapping mode atomic force microscopy (Nanoscope IV Digital Instruments) in the height and phase contrast mode, field emission scanning electron microscopy (FESEM, JEOL JSM-7001F) with an acceleration voltage of 10 kV and high resolution transmission electron microscopy (HRTEM, JEOL 2100F) at 200 kV in the bright field. TEM samples were prepared by drop casting the dispersions on a holy carbon grid, followed by drying under vacuum for 24 h at 50 °C. Selected area electron diffraction patterns were obtained in the HRTEM analysis. Energy dispersive X-ray (EDX) spectra of the TMD/polymer composite films were obtained using an EDX spectrometer by FESEM with an acceleration voltage of 10 kV.

Polymer	Structure	M_n x 10^3	PDI	Tg (°C)	NH_2 Functionality
Polystyrene **PS**	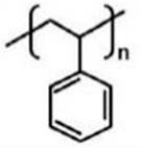	11.5	1.04	90	------
Amine Terminated Polystyrene **PS-NH_2**	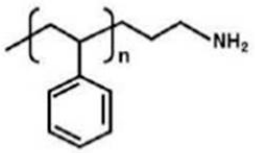	9.5	1.16	102	>98%
		25	1.35	102	>98%
		40	1.05	102	>98%
		108	1.12	102	>98%
Amine Terminated Polymethyl methaccrylate **PMMA-NH_2**	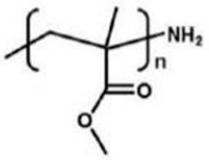	20	1.2	131	>98%
Amine Terminated Polyethylene **PE-NH_2**	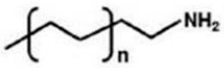	4.2	1.05	None Tm - 102 Tc - 89	>98%
Amine Terminated Polybuda -diene **PBd-NH_2**	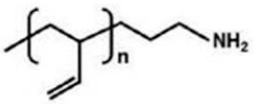	15	1.08	-14	>98%
Amine Terminated Polyethylene Oxide **PEO-NH_2**	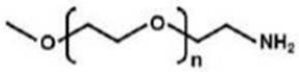	9.5	1.07	No Data	>95%
Amine Terminated Polystyrene-*b*-isoprene **PS-*b*-PI-NH_2**	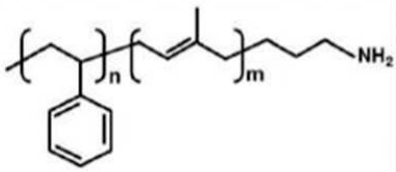	23-*b*-37.5	1.06	No Data	>90%

Table 1. Physical properties of the polymers used in this study

TMDs	Mol.Wt	Size	Density	Supplier	Product Number
Molybdenum (IV) selenide **$MoSe_2$**	253.87	-325 Mesh Powder	6	Alfa Aesar	13112
Molybdenum (IV) sulfide **MoS_2**	160.07	~6 μm	5.06	Sigma Aldrich	69860
Tungsten (IV) selenide **WSe_2**	341.77	~10 μm	9.32	Alfa Aesar	13084
Tungsten (IV) sulfide **WS_2**	247.98	No data	7.5	Alfa Aesar	11829
Rhenium (IV) sulfide **ReS_2**	250.33	No data	7.506	Alfa Aesar	89482
Niobium (IV) selenide **$NbSe_2$**	250.83	~5 μm	No data	Alfa Aesar	13101
Zirconim (IV) telluride **$ZrTe_2$**	346.42	-325 Mesh Powder	6.42	Alfa Aesar	36321

Table 2. Physical properties of the TMDs used in this study

4. Results and Discussion

4-1) Supramolecular π-π interactions
: Exfoliation and dispersion of LIMs with Py-P4VP

Non-covalent functionalization by physical π-π-interactions with LIMs is a promising method because it offers the possibility of attaching functional groups to nanosheets without disturbing the structural and electronic properties. The hexagonal arrangement of the carbon atoms in polymer chain or functional group is isomorphic to graphite like layered BN and TMDs, which shows hexagonal (2H) polymorphs, and thus, π-π-interactions between them is reasonably expected. We examined how π interaction sterically shields attractive forces between the surface of the LIM nanosheets such as BN and MoS_2, the effect on the structure, and properties of both nanosheets and polymers to design the nanoelectronic devices. In fact, the LIM nanosheets were functionalized with P4VP-Py by π- π interaction between pyrene molecule and surface of nanosheet as schematically shown in **Figure 1**, showing the most successful dispersions of the MoS_2 and BN in various solvents such as DMF, ethanol and IPA. As shown in **Figure 1**, all batches using the P4VP derivatives showed characteristic peaks of MoS_2 because the MoS_2 nanosheets were well-dispersed in the polymer solution due to the electron donating and accepting interaction between the amine of 4-VP and d orbital of transition metal. In fact, the batch with the P4VP-Py exhibited the best absorption peak and stable dispersion comparing to the P4VP-C4-amine. It is expected that the planner geometry of pyrene leads the π-π interaction with the 2-dimensional structure of BN and MoS_2, which results in the stable dispersion of nanosheets in organic solvents. (**Figure 2**)

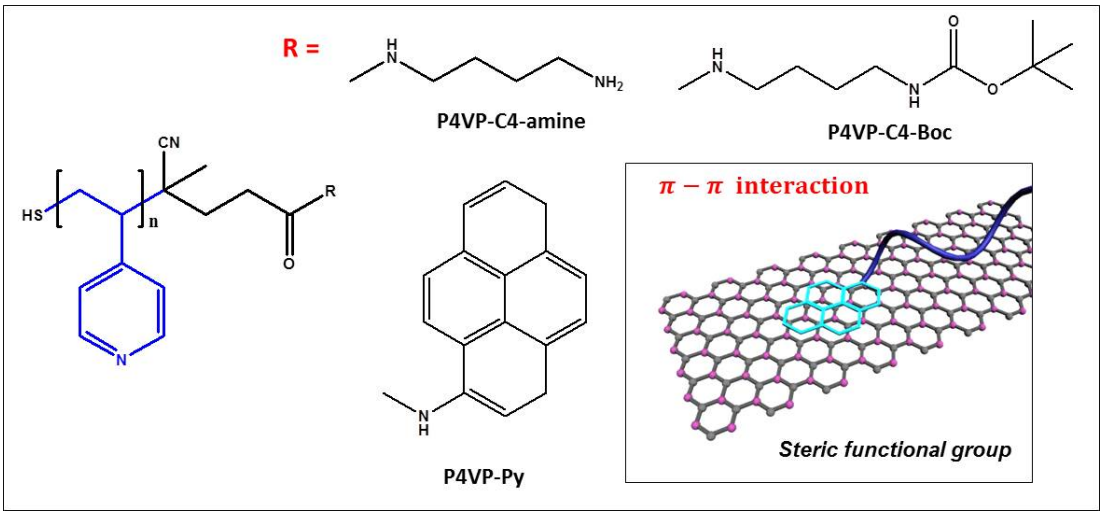

Figure 1. The chemical structures of polymers used in this study for ensuring π-π interaction with LIMs. Scheme representatives the mechanism of the exfoliated LIMs using a pyrene-terminated polymer in an organic solvent.

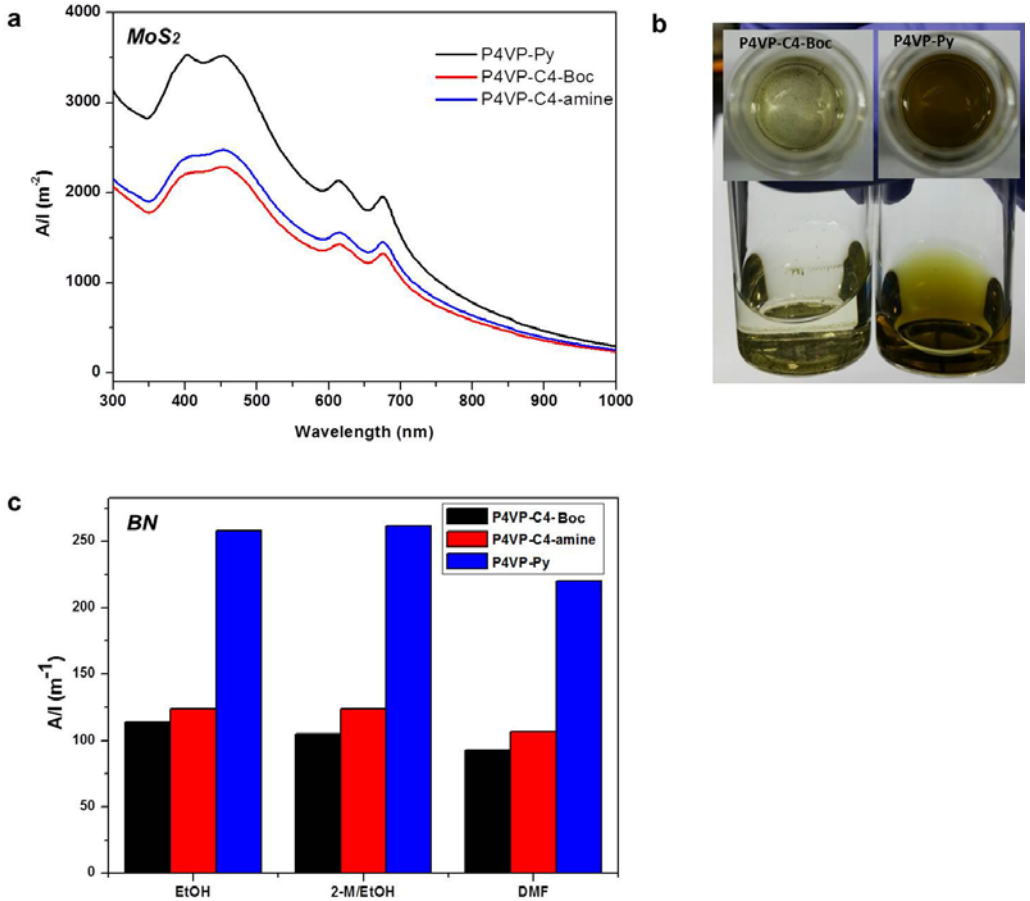

Figure 2. a) Absorbance spectra of MoS_2 composite films dispersed with pyrene (black), C4-Boc (red) and C4-amine (blue) terminated P4VP polymers, respectively. The strongest intensities of MoS_2 peaks at 450, 462, 675 and 734 nm were detected from the P4VP-Py/MoS_2 film, which indicates the well-dispersed nanosheets within the steric end-group terminated polymer. b) Photographs of MoS_2 solutions with P4VP-C4-Boc (left) and P4VP-Py (right) in DMF for comparing the different degree of exfoliation and dispersion as function of end-groups. c) Absorbance intensities at 550 nm of the exfoliated BNs solutions in various organic solvents according to the end-functional groups.

4-2) Electron donating and accepting interaction

End-functionalized polymers with chemical functional groups at the end are promising candidates as model materials because functional groups are expected to strongly interact to the LIMs surface while the polymer provides good solubility in various solvents, polymer matrices. In this approach, numerous combinations of various polymers and functional chemical groups with different polymer chain lengths can be designed, depending upon the chemical nature of different LIMs. For instance, the amine functional groups and metal ions are possible for different types of interactions, (e.g. acid-base interactions). Various polymers such as amorphous, crystalline and elastomeric and insulating, semiconducting and conducting ones are applicable, depending on their final usages.

4-2.1) Universal exfoliation of TMDs with amine-terminated polymers

Our method is based on the non-destructive modification of TMD sheets with amine-terminated polymers. The universal interaction between amine and transition metal resulted in scalable, stable and high concentration dispersions of a single to a few layers of numerous TMDs. We achieved successful exfoliation of numerous TMD nanosheets such as MoS_2, WS_2, $MoSe_2$, WSe_2, ReS_2, $ZrTe_2$ and $NbSe_2$ with amine-terminated polymers. The principle is based on the Lewis-like acid-base interaction between the transition metal and primary amine, as shown in the scheme in **Figure 3**. The representative amine-terminated polymers employed here are glassy PS-NH_2, PMMA-NH_2, rubbery PBd-NH_2, semi-crystalline PE-NH_2, PEO-NH_2 and PS-*b*-PI-NH_2.

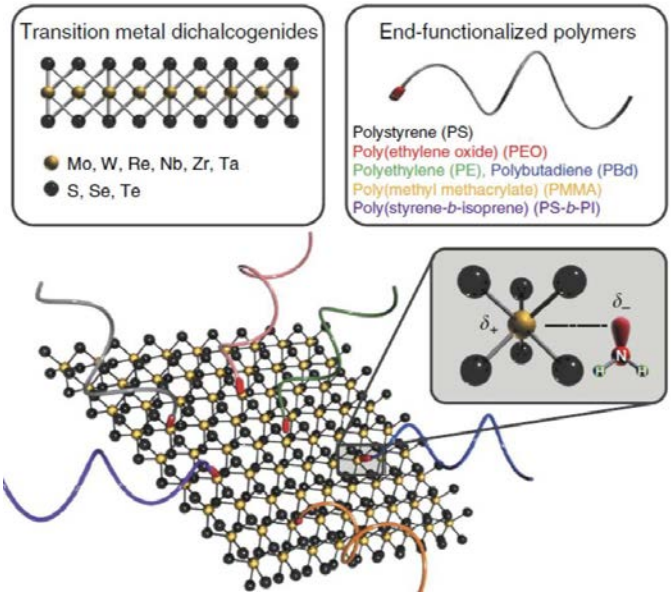

Figure 3. Liquid phase exfoliation of TMDs with end-functionalized polymers. Schematic representation of the proposed mechanism for theexfoliation of various TMDs using different types of amine-terminated end-functionalized polymers in organic solvents. Hexagonal layers of transition metal atoms (M) sandwiched between two layers of chalcogenides (X) are represented by a stoichiometry of MX_2 by the yellow and grey spheres, respectively. The amine-terminated polymers are simplified for clarity. Interaction between the lone electron pairs of nitrogen atoms and the electron-accepting metal atoms weakens the self-layer-layer attraction and the polymer chains provide further separation between the layers, thereby ensuring good exfoliation and dispersion.

We selected $MoSe_2$ and PS-NH_2 as examples and investigated them in detail to demonstrate the effectiveness of our proposed strategy. The interaction between the donated lone pairs of nitrogen atoms and electron-accepting metal atoms was evidenced by Fourier transform infrared

spectroscopic (FT-IR) for model systems (PS-NH_2, $MoSe_2$/PS-NH_2) based on density functional theory (DFT) frequency calculation employing B3LYP functional with LANL2DZ basis set as implemented in Gaussian 09 program. For the sake of simplicity, the PS-NH_2 is modeled as an amine-terminated styrene monomer (H-Styrene-CH_2-NH_2) and the ($MoSe_2$) nanosheet is modeled as a Mo_4Se_8 cluster. The geometries were first optimized in the gas phase and the frequency calculations of the optimized geometries were then performed with the consideration of solvent (toluene) effect using IEF-PCM solvent model. As seen in **Figure 4**, the peak at 1673.94 cm^{-1} for scissoring (bending) vibration of the NH_2 in the absence of $MoSe_2$ is shifted to higher frequency (1684.61 cm^{-1}) in the $MoSe_2$/PS-NH_2 bound state, which consolidates our experimental observation.

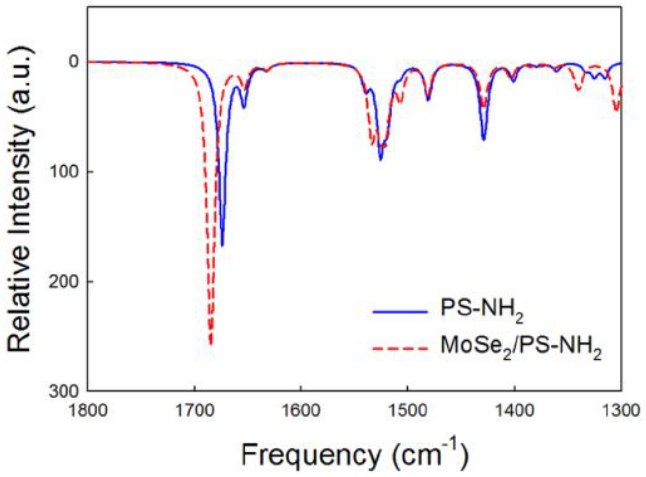

Figure 4. IR simulation spectra of interaction between polymers and TMDs. Comparison of the simulated IR spectra of PS-NH_2 (Blue line) and $MoSe_2$/PS-NH_2 (dotted red line).

Our method is different from metal ions and small molecules intercalation and further sonication assisted exfoliation methods, because there is no intercalation step of TMDs with amine-terminated polymers in our process. It is indeed difficult to imagine that polymer molecules highly swollen in solvent medium with their radius of gyration of approximately a few nanometers are inserted into such a small gap of two stacked nanosheets (~1 nm). The root mean square radius of gyration ($\{\langle s\rangle^2\}^{1/2}$) of the PS-$NH_2$ (9.5 kg/mol) is approximately 4 nm in toluene, based on the equation of $\{\langle s\rangle^2\}^{1/2} = \alpha\,(C_\infty)^{1/2} n^{1/2} l$, where is expansion parameter in toluene, C_∞ characteristic ratio of PS, n the number of bonds and l corresponds to C-C bond length. Instead, amine groups of polymers more efficiently interact with transition metals when surface of TMD nanosheets is exposed upon sonication step and the anchored polymers on the surface of TMDs in turn stabilize the dispersion of nanosheets in solvent.

To confirm our argument, we separated the processes. A solution of bulk $MoSe_2$ in toluene was sonicated without the addition of PS-NH_2 and subsequently mixed with PS-NH_2 solution which had been prepared. (**Figure 5a**) While a solution without polymer was immediately settled down in few minutes, the mixed solution exhibited TMDs well dispersed in toluene. (**Figure 5b**) The quantitative analysis of the dispersion of $MoSe_2$ suggests that no significant difference in the dispersion was observed between single and two step processes, which implies that amine terminated polymers play a role of mainly stabilizing TMD sheets in solvent and preventing them from re-aggregating upon film formation. Another experiment we designed was to examine the dispersion of $MoSe_2$ with PS-NH_2 without sonication step. When a mixture of $MoSe_2$ and PS-NH_2 was gently stirred in toluene, nanosheets were rarely dispersed in solvent as expected. (**Figure 5b**). □

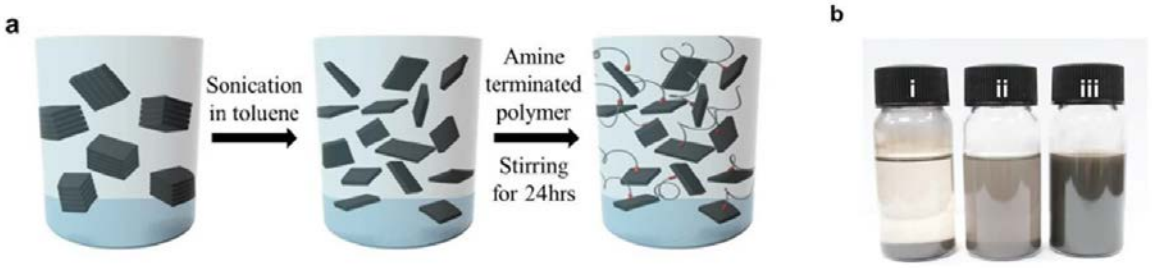

Figure 5. Exfoliation and dispersion of TMDs with end-functionalized polymers. a) Schematic illustration of the proposed mechanism for the exfoliation and dispersion of various TMDs using different types of amine-terminated end-functionalized polymers. A solution of bulk $MoSe_2$ in toluene was sonicated without the addition of PS-NH_2 and subsequently mixed with PS-NH_2 solution (sonicated and mixed solution). Compared to $MoSe_2$ solution sonicated in toluene without polymer and simple mixing of bulk $MoSe_2$ and PS-NH_2 in toluene, which were immediately settled down in few minutes, the sonicated and mixed solution exhibited $MoSe_2$ well dispersed in toluene. b) Photograph of (i) bulk $MoSe_2$ in toluene was sonicated without the addition of PS-NH_2 (ii) simple mixing of bulk $MoSe_2$ and PS-NH_2 in toluene (iii) bulk $MoSe_2$ in toluene was sonicated and subsequently mixed with PS-NH_2 solution.

The (002) peak shift to low theta angle observed due to the efficient intercalation of TMDs by small molecules in the previous study was not, therefore, observed in our process but the (002) peak was substantially reduced in intensity due to highly exfoliated nanosheets separated by intervening polymers. (**Figure 6a and b**) The absorbance spectra of the $MoSe_2$ dispersions obtained under two step process (**Figure 6c**) shows similar characteristic peaks of exfoliated $MoSe_2$ obtained by one step process and other methods without PS-NH_2, confirming the exfoliation and stable dispersion of $MoSe_2$ in toluene by our method.

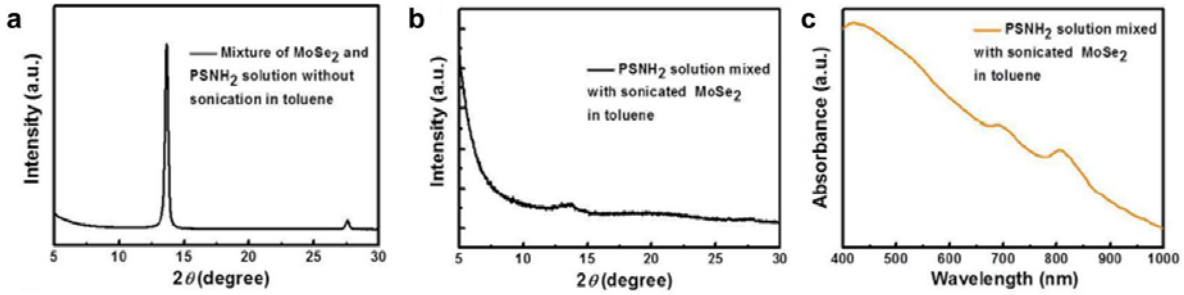

Figure 6. XRD results of c) Mixture of bulk $MoSe_2$ and PS-NH_2 in toluene without sonication and d) bulk $MoSe_2$ in toluene was sonicated and subsequently mixed with PS-NH_2 solution. e) Absorbance spectra of bulk $MoSe_2$ in toluene was sonicated and subsequently mixed with PS-NH_2 solution.

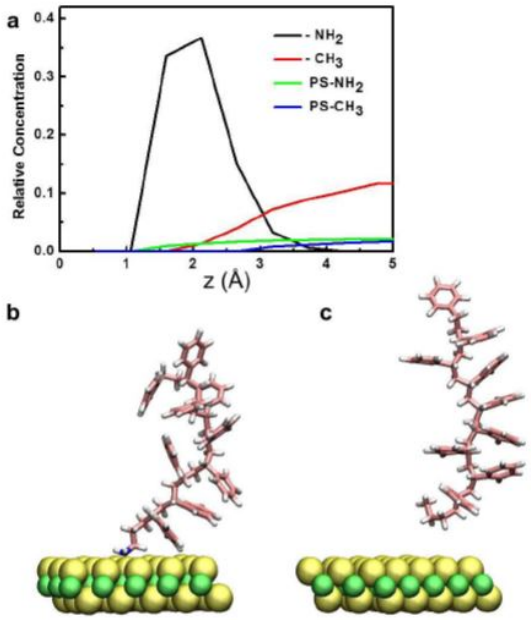

Figure 7. Simulation results of interaction between polymers and TMDs. a, Comparison of the simulated concentration profile of -NH_2,-CH_3, PS-NH_2 and PS-CH_3 in the direction perpendicular to the TMD surface (z). Simulation snapshot of typical conformational states for b, PS-NH_2 and c, PS-CH_3 on the TMD surface.

To further investigate the effect of amine-terminated end-functionalized polymers as a dispersant, we simulate the physic-sorption of amine terminated PS (PS-NH2) and methyl-terminated PS (PS-CH_3) onto TMD (TiS_2) surface using density functional tight binding (DFTB) combined with Born-Oppenheimer molecular dynamics (MD) simulation. Since DFTB parameter sets for Mo and Se interacting with amine were not available in our system, we instead examined a common TMD, TiS2 whose electronic structure is similar to $MoSe_2$. **Figure 7a** compares the simulated concentration profile of PS-NH_2 and PS-CH_3 in the direction perpendicular to the TMD surface (z). The profiles are obtained from the time averaging of MD samples for 5 ps after 10 ps equilibration. The profiles clearly indicates that the amine terminal group are strongly physisorbed onto the surface showing a pronounced peak at ~ 2 angstrom, whereas PS-CH_3 does not show any peak near the surface. This suggests that non-functionalized PS simply wanders away from the surface at the urging of thermal and stirring force while PS-NH_2 can be anchored onto the TMD surface forming brush-like molecular clusters. Two simulation snapshots (**Figure 7b and c**) demonstrate typical conformational states for PS-NH_2 and PS-CH_3 on the TMD surface.

4-2.2) Exfoliation and dispersion of $MoSe_2$ with amine terminated polymers

: Determination of the optimal conditions for dispersion

To demonstrate the effectiveness of our strategy, we extensively investigated the dispersion of $MoSe_2$ nanosheets with PS-NH_2. Initially, the exfoliation of $MoSe_2$ in toluene, which is a poor solvent for $MoSe_2$, was tested with PS, PS-NH_2, and without polymer by tip sonication with a 10-s pulse on and a 5-s pulse off with amplitude of 50% in an ice bath. $MoSe_2$ in neat toluene and with PS began to precipitate immediately after sonication and completely settled down within few minutes, whereas the dispersion with PS-NH_2 became visually non-scattering with a dark brown color and remained stable, which indicates the preferential attraction between $MoSe_2$

and the amine groups of PS-NH_2. The results prove that PS-NH_2 can enhance the dispersion of the exfoliated nanosheets in non-solvents of $MoSe_2$. (**Figure 8a**)

In order to optimize the dispersion conditions, we further investigated the $MoSe_2$ dispersions in detail in terms of the sonication time, initial $MoSe_2$ concentration, and centrifugation rate with 1 mg/mL PS-NH_2 (**Figure 8b-f**). The quality of the exfoliation and dispersion was initially determined by the absorbance per unit length, A/l, using UV-vis spectrometry. The optimized dispersion conditions were sonication for 45 min with an initial concentration of 10 mg/mL bulk $MoSe_2$, followed by centrifugation at 1,500 rpm for 30 min. The absorbance spectra of the $MoSe_2$ dispersions obtained under these conditions are shown in Figure 2a. Different from pure PS-NH_2, discernible peaks were observed at 800 and 690 nm, which are similar to the characteristic peaks of exfoliated $MoSe_2$ obtained by other methods without PS-NH_2, confirming the stable exfoliation and dispersion of $MoSe_2$ in toluene

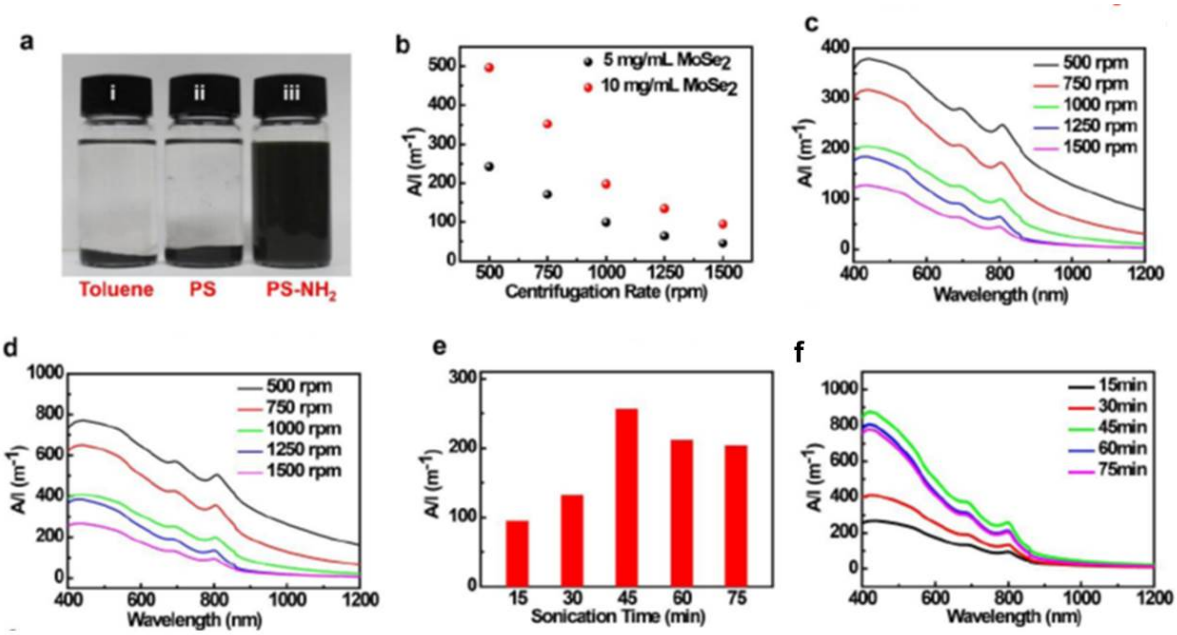

Figure 8. Optimization of the $MoSe_2$ dispersions with PS-NH_2. a) Photographs of the $MoSe_2$ dispersion in toluene (i) without any dispersant, (ii) with PS, and (iii) with PS-NH_2. b) Effect of the centrifugation rate on the $MoSe_2$ dispersion. Absorbance spectra of two different initial $MoSe_2$ concentrations were evaluated: c, 5 mg/mL and d) 10 mg/mL. Sonication time was 15 min. e) Effect of the sonication time and f) the corresponding absorbance spectra of $MoSe_2$ dispersion in toluene. For all of the sonication times evaluated, the initial concentrations of $MoSe_2$ and PS-NH_2 were kept constant at 10 and 1 mg/mL, respectively, and the solutions were centrifuged at 1,500 rpm for 30 min.

: Characterization of $MoSe_2$ dispersion with PS-NH_2

The interaction of amine groups of PS-NH_2 with $MoSe_2$ and the resulting exfoliation into nanosheets was confirmed by X-ray diffraction (XRD) analysis, Raman spectroscopy, and X-ray photoelectron spectroscopy (XPS) and. The XRD patterns of bulk $MoSe_2$ and $MoSe_2$/PS-NH_2 are shown in the Supplementary **Figures 9a** and **b**. The abrupt decrease and broadening of the (002) reflection in the XRD patterns of $MoSe_2$/PS-NH_2 indicates that $MoSe_2$ was exfoliated into a few layers with different dimensions. The Raman spectra of $MoSe_2$/PS-NH_2 deposited on the SiO_2 substrate were compared with the spectra of bulk $MoSe_2$ (**Figure 9c**). The exfoliated $MoSe_2$ nanosheets with PS-NH_2 showed characteristics out-of-plane A1g and in-plane E2g1 Raman modes at 239 and 287.5 cm^{-1}, respectively. These values are consistent with results reported for monolayer $MoSe_2$. The observed characteristic out-of-plane A1g mode at 239 cm^{-1}, not be

observed in 1T-$MoSe_2$, indicates the 2H polymorph structure of the exfoliated $MoSe_2$ nanosheets. In addition, the peak at about 221 cm^{-1}, associated to a distorted 1T phase, is absent, again indicative of the 2H phase.

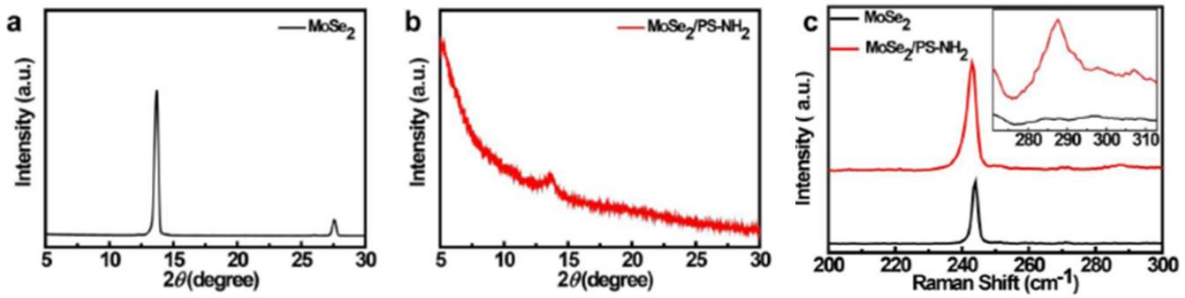

Figure 9. XRD characterizations of a) bulk $MoSe_2$ and b) exfoliated $MoSe_2$ nanosheets with PS-NH_2. c) Raman spectra of bulk $MoSe_2$ and $MoSe_2$/PS-NH_2.

The XPS spectra of the $MoSe_2$/PS-NH_2 confirm the stoichiometry of $MoSe_2$ (**Figure 10a-c**). The two characteristic peaks at 228.8 and 232 eV are attributed to the doublet Mo 3d5/2 and Mo 3d3/2 binding energies, respectively, for Mo4+. The peaks corresponding to the Se 3d5/2 and Se 3d3/2 orbitals of divalent selenide ions (Se2–) are observed at 54.4 and 55.2 eV, respectively. These XPS signals are consistent with values reported elsewhere, corroborating the formation of defect-free $MoSe_2$. The N1s spectrum of PS-NH_2 was deconvoluted into three individual peaks, which are assigned to N– (398.48 eV), –NH– (399.38 eV), and –NH_2 (399.78 eV). These peak positions of the N1s spectrum were shifted after interaction with $MoSe_2$. The binding energies for N–, –NH–, and –NH_2 were shifted to 399.08, 399.78, and 400.48 eV, respectively. The shift of the binding energy of –NH_2 is due to the effect of the interaction between the Mo ions and the donating lone pair electrons of –NH_2.

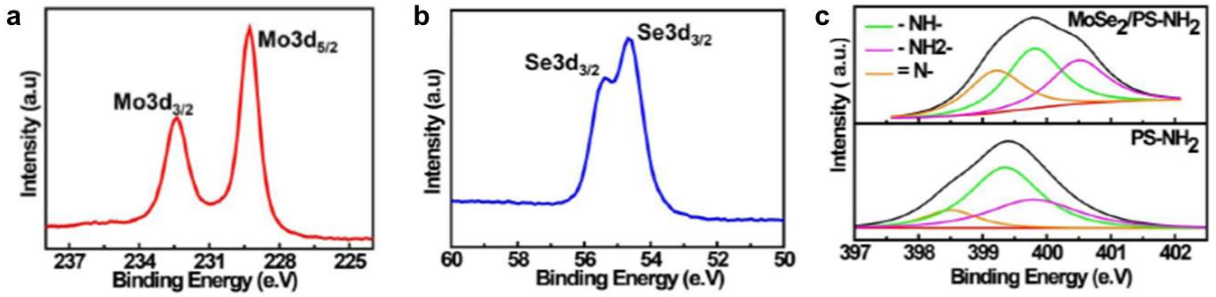

Figure 10. XPS of the $MoSe_2$ nanosheets exfoliated with PS-NH_2. a) Mo 3d spectrum, b) Se 3d spectrum, and c) N 1s spectra of PS-NH_2 and $MoSe_2$/PS-NH_2.

: Effect of the molecular weight of PS-NH_2 on $MoSe_2$ dispersion

The effect of the molecular weight of PS-NH_2 on the $MoSe_2$ exfoliation was also investigated with four different molecular weights (9.5 k, 25 k, 40 k, and 108 k g mol^{-1}) of PS-NH_2. The initial concentration of PS-NH_2 was kept constant at 1 mg/mL and the final concentration of exfoliated $MoSe_2$ was measured (**Figure 11**). As expected, the effectiveness of PS-NH_2 in exfoliation decreases with increasing molecular weight of PS-NH_2. The steric hindrance resulting from the entangled conformations of high molecular polymer chains decreases the reactivity of amine groups and restricts the mobility of the polymer chains in the solvents. Therefore, the

lower the molecular weight of PS-NH_2, the more favorable the amine interactions and thus, better exfoliation and dispersion of $MoSe_2$ nanosheets occurs. PS-NH_2 with a molecular weight of 9.5 kg/mol was further utilized for all of the analyses.

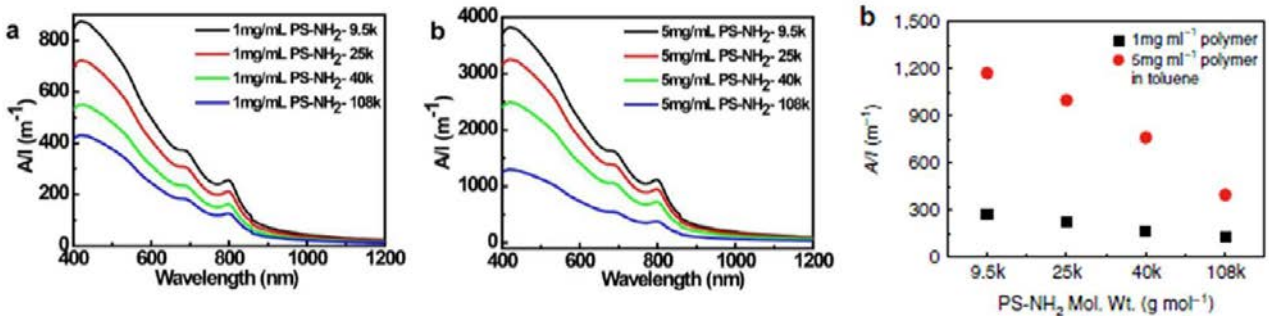

Figure 11. Effect of the PS-NH_2 molecular weight on the $MoSe_2$ dispersion. Absorbance spectra of $MoSe_2$ dispersions depending on PS-NH_2 with different molecular weights for initial polymer concentrations of a) 1 mg/mL, and b) 5 mg/mL. c) Effect of the molecular weight of PS-NH_2 on the efficiency of the $MoSe_2$ dispersion in toluene characterized by the absorbance values of the dispersions at 800 nm. The initial concentrations of $MoSe_2$ and PS-NH_2 were kept constant at 10mg/mL and 1mg/mL, respectively, for all of the molecular weights of PS-NH2 evaluated. Increasing the molecular weight of PS-NH_2 leads to a decrease of the efficiency of the $MoSe_2$ dispersion.

: Determination of the concentrations

The concentration of the dispersed $MoSe_2$ nanosheets with PS-NH_2 in toluene was determined by a traditional gravimetric method. A precisely measured volume of the $MoSe_2$ dispersion was poured into a crucible and the solvent was removed in a vacuum oven overnight. Then, the mass of the crucible was measured and used to determine the concentration of $MoSe_2$ in the dispersion according to the following **equation (1).**

$$Concentration = \frac{Final\ crucible\ mass - Initial\ crucible\ mass\ (mg)}{Volume\ of\ the\ solvent\ (mL)} \quad \ldots\ldots\ldots\ldots\ldots\ldots\ldots \quad (1)$$

TGA was utilized to determine the dispersed amount of $MoSe_2$ nanosheets in the PS-NH_2-modified $MoSe_2$ composite (**Figure 12**). From the TGA results of the PS-NH_2-modified MoSe2 composite, the quantity of the MoS_e2 nanosheets was estimated to be 26%, which allowed us to determine the final concentration of the MoSe2 nanosheets in the dispersion without PS-NH_2 to be 0.22 mg/mL. The extinction coefficient ($\propto$) of the $MoSe_2$ nanosheets with PS-NH_2 in various organic solvents was determined using the Lambert–Beer law.
(**Equation 2 and 3**)

$$\boldsymbol{A = \propto lc} \quad \ldots\ldots\ldots\ldots\ldots\ldots\ldots\ldots\ldots\ldots \quad (2)$$

$$\propto = \boldsymbol{A/lc} \quad \ldots\ldots\ldots\ldots\ldots\ldots\ldots\ldots\ldots\ldots \quad (3)$$

Here, A is the measured absorbance, l is the cell length, and c is the dispersed concentration.

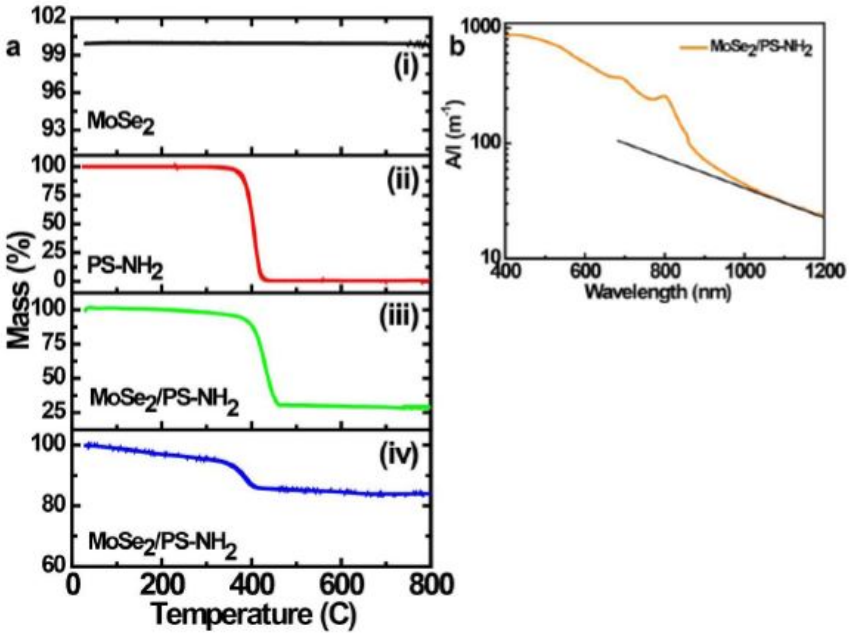

Figure 12. Determination of the $MoSe_2$ concentration. a) Thermogravimetric analysis for (i) the $MoSe_2$ powder, (ii) PS-NH_2, (iii) $MoSe_2$ modified with PS-NH_2, and (iv) after removing the excess PS-NH_2 at 15,000 rpm for 90 min in the $MoSe_2$ dispersion. b) Absorbance spectrum of the $MoSe_2$ dispersion with 1 mg/mL PS-NH_2 on the log scale.

The samples were controllably diluted in series and the absorbance per unit length (A/l) as a function of the $MoSe_2$ concentration was measured. The background scattering illustrated by the line in the plot of the absorbance spectrum of $MoSe_2$ with PS-NH_2 (**Figure 12b**) was subtracted from the spectrum. The background subtracted A/l value at 800 nm was plotted as a function of the $MoSe_2$ concentration (**Figure 13a**) and the A/l values linearly increased with increasing measured concentration. The calculated absorption coefficient (α) was determined from the slope of the curve to be 932 L g^{-1} m^{-1}, which was used to determine the concentrations of the further dispersions.

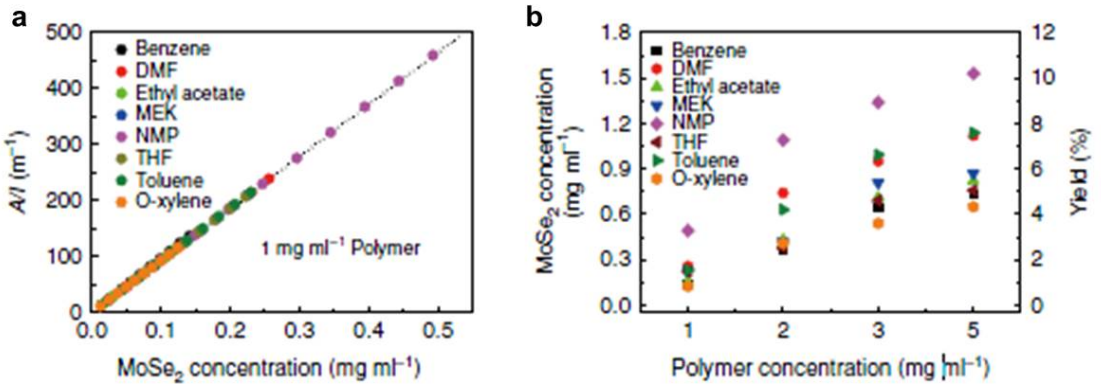

Figure 13. (a) Absorbance at a wavelength of 800 nm as a function of the $MoSe_2$ concentration in each solvent. The absorbance linearly increased with the amount of $MoSe_2$ following Lambert–Beer behaviour, which implies uniform dispersion of $MoSe_2$ without aggregation in all of the solvents. (b) Plots of the concentration of $MoSe_2$ as a function of the initial concentration of PS-NH_2 in different organic solvents. Yield of one to three layers (70%) of the exfoliated $MoSe_2$ nanosheets with PS-NH_2 as a function of the initial concentration of PS-NH_2 in different organic solvents are also shown.

: $MoSe_2$ dispersed with PS-NH_2 in various solvent media

The absorbance variations of the $MoSe_2$ dispersions were measured at an excitation wavelength of 800 nm with 1 mg/mL PS-NH_2 as a function of the $MoSe_2$ concentration in each solvent (**Figure 14**). The absorbance linearly increased with the amount of $MoSe_2$ in accordance with Lambert-Beer behavior and the results imply that the $MoSe_2$ nanosheets are uniformly dispersed without aggregation in all of the solvents.

We further investigated important dispersion properties such as the maximum amount of $MoSe_2$ dispersed in a solvent and the amount of PS-NH_2 required for $MoSe_2$ dispersion at a certain concentration dependent upon the solvent (**Figure 15**). The dispersed $MoSe_2$ concentration increased monotonically with increasing PS-NH_2 concentration due to the increase of reactive amine functional groups.

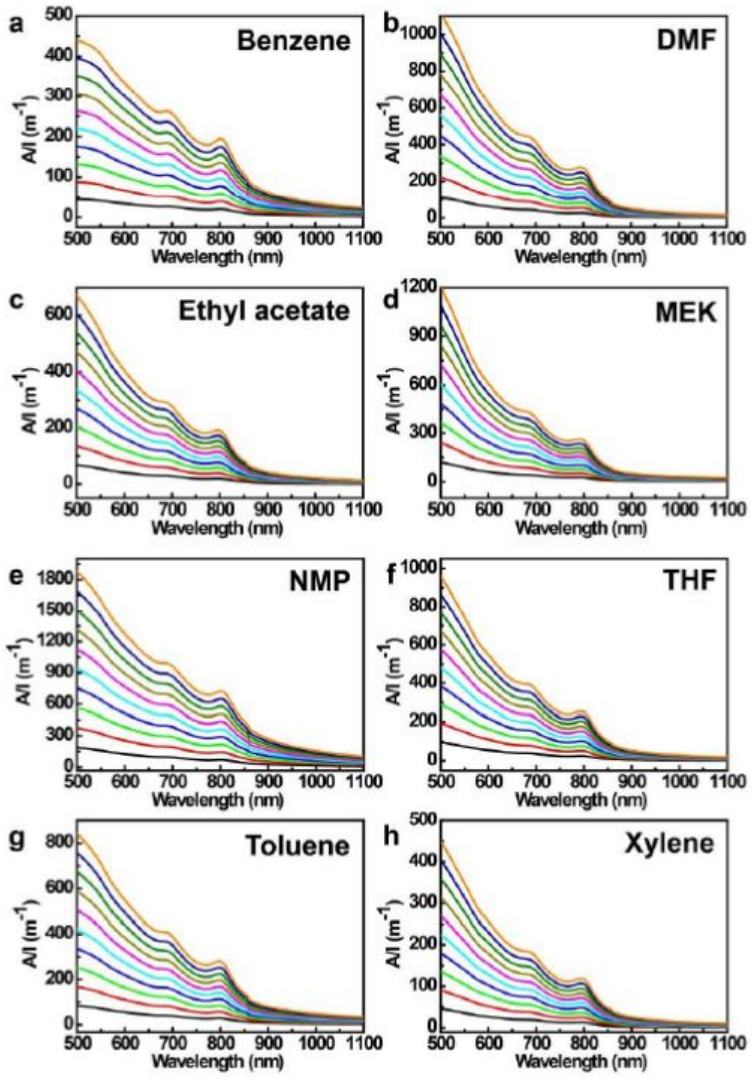

Figure 14. MoS_{e2} dispersion in various solvents. Absorbance spectra of the series of diluted $MoSe_2$ dispersions with 1 mg/mL PS-NH_2 in various solvents.

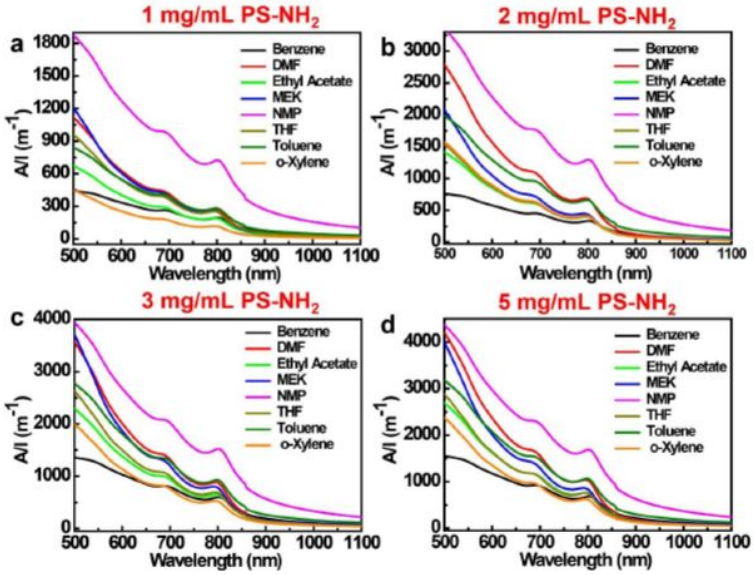

Figure 15. $MoSe_2$ dispersions with different PS-NH_2 concentrations. Absorbance spectra of $MoSe_2$ dispersions in various solvents as a function of the PS-NH_2 concentrations.

: Stability of $MoSe_2$ dispersed with PS-NH_2

The stability of the $MoSe_2$ dispersions after centrifugation in solvents with 5 mg/mL PS-NH_2 was monitored by optical absorbance at 800 nm as a function of time, as shown in **Figure 16**. The absorbance of the $MoSe_2$ dispersions did not significantly change, indicating that the dispersed $MoSe_2$ was highly stable without re-aggregation and sedimentation for a period of more than 3 weeks. The high-concentration dispersion and long-term stability of $MoSe_2$ can be ascribed to the strong interaction of the amine groups with the $MoSe_2$ nanosheets as well as the long and flexible chains of polymers, which provide good solubility in various solvents.

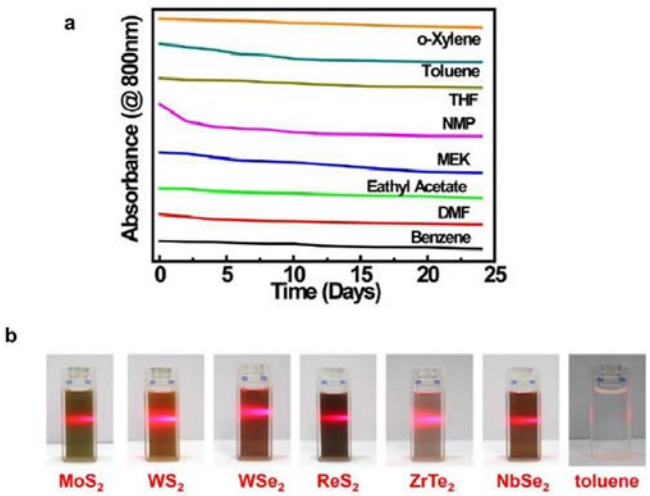

Figure 16. a) Stability of dispersed $MoSe_2$. Absorbance of $MoSe_2$ dispersions measured at 800 nm in various solvents with 5 mg/mL PS-NH_2 as a function of time. The absorbance results are vertically shifted for clarity. b) Exfoliation of the different TMDs with PS-NH2. Photographs of different TMDs dispersed in toluene with 1 mg/mL of PS-NH_2. All of the dispersions were diluted to observe variations of the color. A red laser beam was directed through the TMD dispersions to show the Tyndall effect of the colloidal solutions. For comparison, pure toluene is also known

The large amount of PS-NH_2 in the PS-NH_2-modified MoS_{e2} composite may not be suitable for subsequent electronic applications due to the intrinsic insulating properties of PS-NH_2. To remove the excess amount of the non-interacted PS-NH_2 in the dispersions, the dispersions were centrifuged for 90 min at 15,000 rpm. The precipitate was collected and dried to remove the solvents.

: Morphology of the MoSe2 nanosheets

The microstructures of the exfoliated nanosheets were investigated using both surface probe and electron microscopy, where the results show that the thickness of the single-layer $MoSe_2$ was 1.0±0.15 nm, which is thicker than that of pristine $MoSe_2$ (B0.7 nm) due to the attached polymer chains on both sides of the nanosheet. The single crystalline nature of the single- and few-layer $MoSe_2$ was preserved during the exfoliation process as well (**Figure 17**)

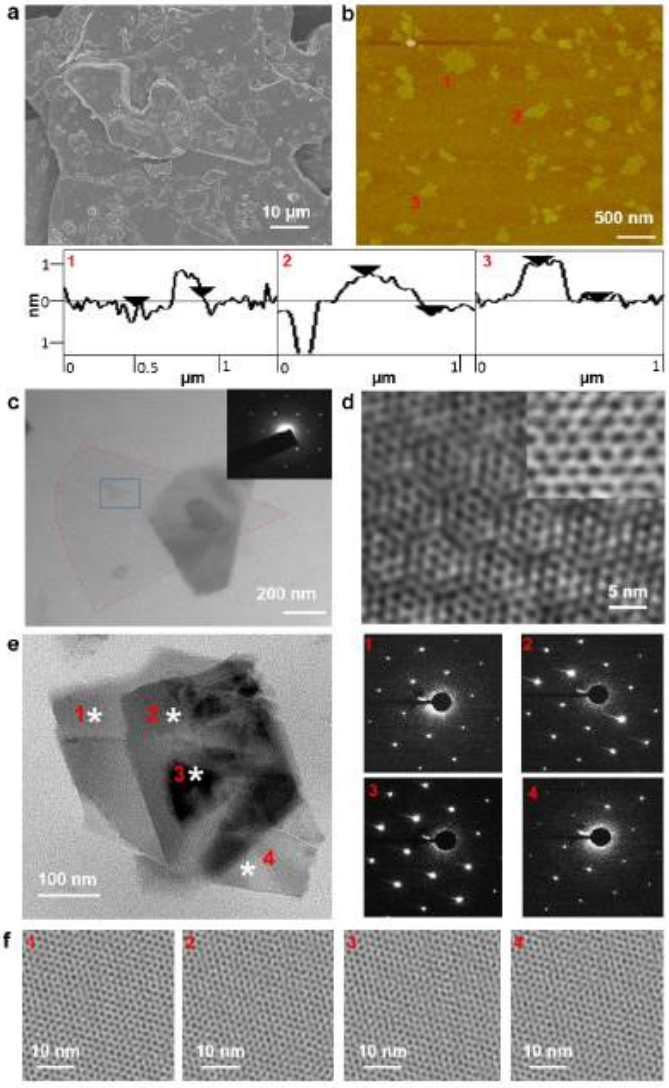

Figure 17. Morphology of the $MoSe_2$ nanosheets. (a) SEM image of bulk $MoSe_2$ powder. (b) Tapping mode AFM micrograph along with height profile of distribution of exfoliated $MoSe_2$ nanosheets in toluene spin-coated on a Si substrate. The height profile measured in clearly shows a monolayer $MoSe_2$ sheet with a thickness of approximately 1.0 nm. (c) Bright field TEM image of single- and few-layer $MoSe_2$ nanosheets. The inset shows the selected area electron diffraction (SAED) pattern of a $MoSe_2$ nanosheet. (d) High resolution TEM (HR-TEM) image of the $MoSe_2$ nanosheets. The digitally filtered image in the inset clearly shows hexagonal symmetry of the $MoSe_2$ nanosheets.

The SAED pattern and HR-TEM collected from the marked box region. (e) Bright field TEM image of few-layer $MoSe_2$ nanosheets and different thickness regions marked with numbers and their corresponding SAED patterns. (f) HR-TEM images of different regions.

As expected, bulk and many layers of $MoSe_2$ nanosheets prepared by low centrifugation rate do not exhibit any noticeable PL. In addition, electron microscopy results of both bulk and exfoliated TMDs including MoS_2, WS_2, WSe_2, ReS_2, $ZrTe_2$ and $NbSe_2$ with PS-NH_2 in toluene evidence the universality of our method (**Figure 18**). Statistical analysis of various samples with different centrifuge rates shows that the mean number of layers decreases with the rate and at an optimized condition, a few layered TMDs dispersion was obtained as shown in **Figure 19**.

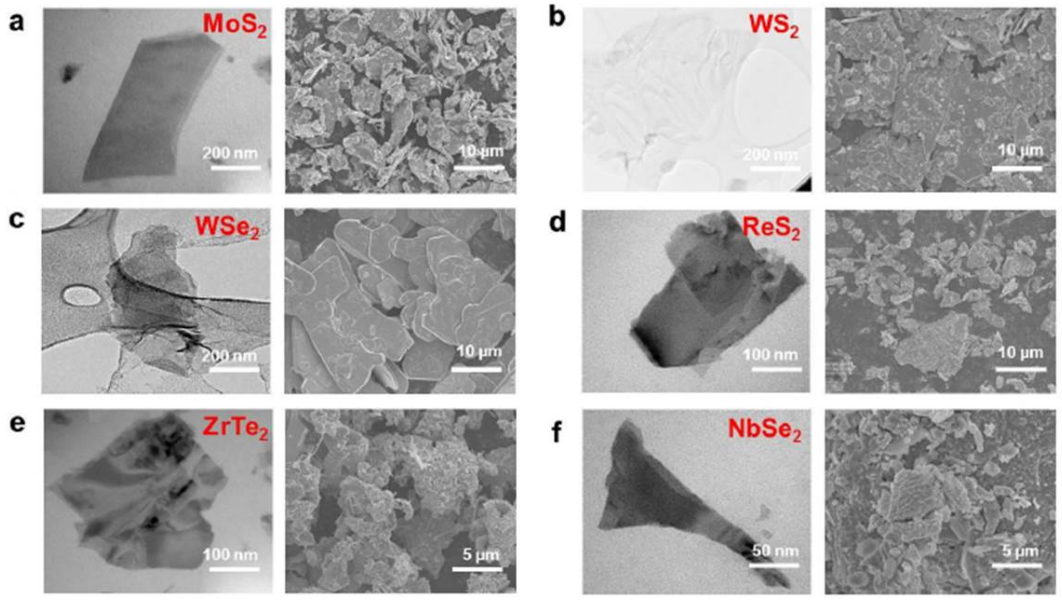

Figure 18. Morphology of the TMD nanosheets. Bright field TEM images of the different exfoliated TMD nanosheets and SEM images of bulk TMD powders.

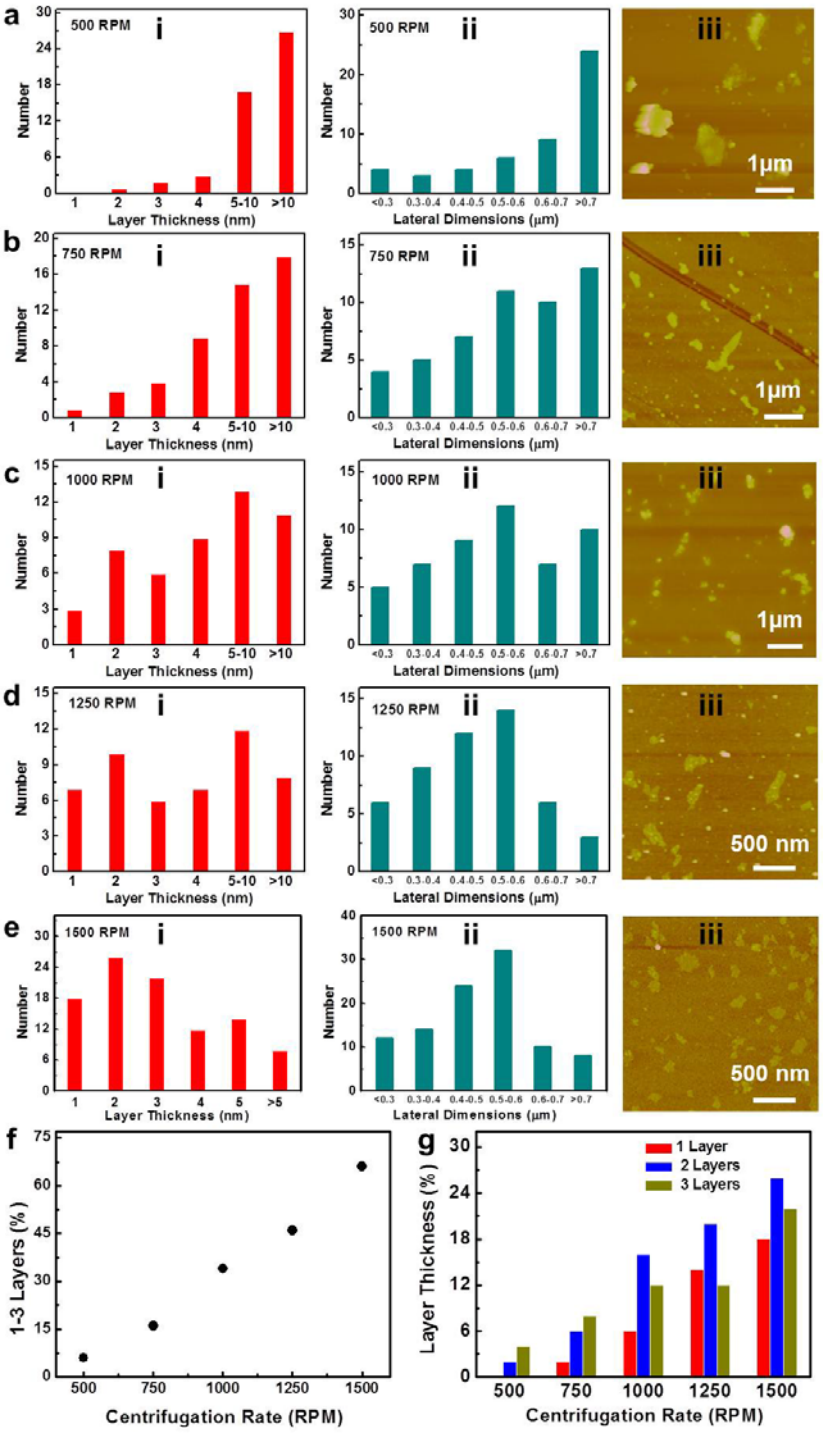

Figure 19. Histograms showing a)-e) (**i**) the average layer thickness, and (**ii**) the average size distribution and (**iii**) representative AFM images of the exfoliated $MoSe_2$ nanosheets at different centrifugation rates. f) Percentage of 1-3 layers and g) distribution of the 1-3 layers of the exfoliated $MoSe_2$ nanosheets as the function of centrifugation rate.

<List of Publications and Significant Collaborations that resulted from your AOARD supported project>

1) Publications

1. D.B. Velusamy, R. H. Kim, S. Cha, J. Huh, R. Khazaeinezhad, S. H. Kassani, G. Song, S. M. Cho, S. H. Cho, I. Hwang, J. Lee, K. Oh, H. Choi, C. Park, "Flexible transition metal dichalcogenide nanosheets for band-selective phododetection", *Nature Communications*, doi:10.1038/ncomms9063, published on 02 September **2015**.
2. K. L. Kim, W. Lee, S. K. Hwang, S. H. Joo, S. M. Cho, G. Song, S. H. Cho, B. J. Jeong, I. Hwang, J. H. Ahn, Y. –J. Yu, S. K. Kwak, S. J. Kang, C. Park, "Epitaxial growth of thin ferroelectric polymer films on graphene layer of fully transparent and flexible nonvolatile memory", *Nano Letters*, submitted on 23 September **2015**

2) Presentations

1. The 13th International Nanotech Symposium & Nano-Convergence Expo NANO KOREA 2015, July 1~3, 2015, Coex, Seoul, Korea. "Solution processible $MoSe_2$ thin films with end functionalized polymers for high performance flexible phododetectors" by Dhinesh Babu Velusamy, **Oral presentation**
2. International Conference on Electronic Materials and Nanotechnology for Green Environment ENGE 2014, November 16-19, 2014, Ramada Plaza, Jeju Hotel, Jeju, Korea. "Solution processible MoS2 thin film photodetectors with polymers" by Dhinesh Babu Velusamy and Cheolmin Park, **Poster presentation**
3. **AFRL On-site seminar**, September 17, 2015 "Controlled interactions between two dimensional layered inorganic nanosheets and polymers", through Window On Science (WOS) Program

3) Interaction with Air Force

Official invitee and presentation speaker of the AF related meeting, named On Site Discussion of Research Collaboration with AFRL, on September 17-19 2015, entitled "Controlled interactions between two dimensional layered inorganic nanosheets and polymers", through **Window On Science (WOS) Program** for promoting collaborations with Air Force researchers, including discussion of two dimensional layered inorganic materials and progress for planned/ongoing projects.

- One hour presentation at AFRL about the recent research related to the grant of the Basic research for AOARD 144054 entitled "Controlled Interactions between Two Dimensional Layered Inorganic Nanosheets and Polymers".
- The meetings (30 min. each) with 12 AFRL experts in material science and shared common research interests.
- Setting up future research collaboration in the field of 2D materials and their photo-electronic applications. In particular, research collaboration with Dr. McConney's group on the subject of the electrical characterization of TMD films grown in AFRL as well as epitaxial growth of functional polymers on the TMD films.